Journal of the Southeastern Association for Research in Astronomy, **5**, 2-7, 2012 February 1

MODELING BINARY CENTRAL STARS OF PLANETARY NEBULAE I: HF 2-2

Samuel Clay Schaub[1]
Department of Physics and Astronomy, Valparaiso University, Indiana, 46383

and

Eva H. L. Bodman[1]
Department of Physics, Syracuse University, New York, 13244

and

Todd C. Hillwig
Department of Physics and Astronomy, Valparaiso University, Indiana, 46383

ABSTRACT

In our quest to understand the shaping mechanisms of planetary nebulae (PNe), we have modeled the known binary central star Hf 2-2. The models have been matched to photometric variation data in B, V and R filters. Our goal was to constrain as much as possible the fundamental properties of the binary system: the masses, temperatures, and radii of each star as well as the inclination angle of the system. These constrained system properties, especially the inclination angle, can then be compared with the predictions of the theory that binary stars are responsible for the complex shapes we see in PNe. The inclination angle for Hf 2-2 has been constrained to the range of 25°-55°. From visual inspection of the nebula, the inclination angle range of Hf 2-2 includes alignment with the nebula, though thorough modeling of the nebular structure is necessary to draw an unambiguous conclusion.

Subject headings: binaries: close, planetary nebulae: Hf 2-2, stars:variable:other

1. INTRODUCTION

1.1. *General Background*

Planetary nebulae (PNe) are the photoionized gases and dusts that were shed by an intermediate mass star in the Asymptotic Giant Branch (AGB) and proto-planetary nebular (proto-PN) stages of stellar evolution. The central stars of PNe are very hot, dense former stellar cores contracting to the white dwarf cooling track, if they are not already white dwarfs. PNe form expansive, colorful, and intricate structures as the last gasps of dying, intermediate mass stars(cf. Kwok 2007).

At first thought, one would naively expect PNe to be primarily spherical in shape, as they are the resultof mass loss from spherical stars. Perhaps some equatorially concentrated mass loss due to rotation of the star could impart some elliptical shaping to the structure, but nothing far different from a sphere. An early accepted model for the formation of such nebulae is described in the Interacting Stellar Winds (ISW) model, (Kwok et al. 1978). Mass lost during and shortly after the AGB phase is carried away by slow stellar winds of the order of 10 km/s at a rate of up to 10^{-5} $M_\odot$ yr^{-1}. During the proto-PN and PN phases, mass loss has dropped to 10^{-8} $M_\odot$ yr^{-1}, but the stellar wind can reach speeds in excess of 1000 km s^{-1} (Balick and Frank 2002). The fast stellar winds quickly overtake and sweep up the slower, denser material lost during the AGB phase. From this picture, we should expect to see PNe consisting of nearly evacuated central cavities separated from a smooth halo of slow winds by a bright, generally spherical shell of gases plowed up by the fast stellar wind. Frank, Balick, & Riley (1990) demonstrated agreement with observed density distribution in round PNe and the predictions of the ISW model.

While round PNe are seen in the sky, they are not the only shapes we observe, nor are they even the most common. PNe are seen to exhibit bipolar, point-symmetric, and axisymmetric shapes. Bipolar PNe display two lobes on opposite sides of the central star, often constricted by a narrow waist at the minor axis of reflection symmetry. The complex filamentary structure of point-symmetric nebulae is characterized by very similar nebulae structures directly opposite each other with respect to the geometric center. Axisymmetric nebulae display reflection symmetries about one or more axes. These more complex symmetries are beyond the explanatory scope of the ISW model.

The mechanisms that shape PNe have been proposed to be due to the torques of binary stellar systems or magnetic fields. No single mechanism can explain all of the various shapes observed. However, a generalized interacting stellar winds (GISW) model has been proposed that seems to account for the bipolar nebulae, as well as some ellipsoidal shapes, (Balick and Frank 2002). In the GISW model, a relatively dense, dusty torus forms around the central star during the AGB and proto-PN phase. This then funnels the expansion of the fast stellar wind of the PN phase, creating a two-lobed structure. An opaque waste is seen in many bipolar PNe, and a torus has even been imaged surrounding proto-PNe (Kwok et al. 2000). The GISW successfully accounts for at least the basic structure of many of the more exotically shaped PNe.

What is lacking in the GISW, however, is an explanation of the source of the torus. Precisely what mechanism leads to this concentration of material? One proposed explanation is that the torus is due to a close binary stellar system gravitationally concentrating outflowing material into its orbital plane; for a more detailed explanation

Electronic address: sam.schaub@valpo.edu
[1] Southeastern Association for Research in Astronomy (SARA) NSF-REU Summer Intern

of how a binary system can shape a forming PNe, see De Marco (2009). This has led to a variety of searches for close binary central stars of PNe, (Schaub & Hillwig 2009; Miszalski et al. 2009; Bond & Murdin 2000), and dozens of such stars have been found to date. However, little modeling of the actual stellar systems has yet been done. (For a summary of known close binary systems, see (De Marco, Hillwig, & Smith 2008)). It is not enough to know that close binary central stars exist. It must be demonstrated whether or not these are truly correlated with the shape of the nebula. If many of these systems can be well modeled, such correlations could be sought to support or refute the binary hypothesis. A simple example would be to examine the alignment of the axes of orbital rotation with the axes of the PNe. A very high occurrence of alignment would strongly suggest that the binary system is a main shaping force in the formation of the PNe, while a seemingly random distribution would bring a shadow of doubt to the binary hypothesis and fuel the search for other shaping mechanisms.

1.2. *Published Knowlegde of Hf 2-2*

The PN Hf 2-2 is a faint planetary nebula located in the galactic bulge, discovered in 1953 (Hoffleit 1953). Many studies of the nebula have been performed over the years. The optical extinction constant for this nebula is c = 0.73 (Stasińska et al. 1991). The published size of the nebula ranges from 18.5″(Stasińska et al. 1991) down to 17″ in Frew (2008). This range shows the rather subjective nature of such a measurement. The corrected Hβ flux is listed as 12.3 ergs/s/cm (Stasińska et al. 1991). Liu (2003) gives us three different temperature values of : T_e(HeI) = 775, T_e(HI BJ) = 900, and T_e(O III) = 8820, all from recombination lines. Temperature fluctuations across the structure of the nebula are likely responsible for the variation in the measurements. Finally, Hf 2-2 has been identified as having a multiple shell morphology (Miszalski et al. 2009). See figure one for a false-color image.

Moving on to the central star, Liu et al. (2006) published a temperature of 64,000 K to 67,000 K as determined by the Zanstra method using HeII lines. The apparent V magnitude of the central star is 17.37 with an absolute V magnitude of 3.31 (Frew 2008). The central star resides approximately 2900 pc from Earth (Frew 2008). The central star was found to be variable, utilizing MACHO data, with a period of 0.39851 days (Lutz et al. 1998).

2. DATA

The photometric data for Hf 2-2 was was largely comprised of data from the MACHO survey, supplemented with our own observations. Our observations were performed on the 0.9 m telescope at CTIO on the nights of May 17th through May 19th, 2009. The target was imaged using Bessel V, and R filters. The images were calibrated using standard procedures in the *IMRED* package in the IRAF software suite. Aperture photometry was performed using the *DIGIPHOT* package.

Data in the B filter were entirely from the MACHO survey. The data were initially folded on the published period of 0.39851 days. Nine data points that were many standard deviations from the bulk of the data were eliminated. The *PDM* package in IRAF was then used to determine the best period with which to fold the data for modeling. The period of minimum dispersion was 0.39875 days, and this is what was used in the creation of the B light curves presented in this report. The data were to be modeled using Binary Maker 3, and much of the analysis of "goodness of fit" was performed purely by eye. Because of this, the data were binned into 35 phase bins evenly dispersed between 0.0 and 1.0. The data within each bin were combined via a weighted average, and the uncertainty associated with the value in each bin was propagated accordingly from the sigmas reported with each data point from the MACHO survey.

FIG. 1.— This is a figure of the planetary nebula Hf 2-2. The central star can be seen in the geometric center of the image (Schwarz et al. 1992).

Data in the V filter were entirely from our own observations. As our V observations spanned a rather short time, no attempt was made to refine the period with this data. These data were folded on a period of 0.39875 days, just like the B filter. As these data displayed both relatively little scatter, and relatively few data points, no binning was performed on the V data.

Data in the R filter were made of a combination of MACHO data and our own observations. To combine the data, the zero point of our instrumental magnitudes needed to be shifted to match that of the MACHO survey. To facilitate this, both data sets were folded on the published 0.39851 day period, and a sine curve with a floating zero point was fit to each. Our instrumental magnitudes were then shifted using the difference between the zero points of the two fits. The data were then combined, and it was attempted to again use the *PDM* package in IRAF to determine the period of minimum dispersion. The large time gap in the data, however, prevented the software from determining an appropriate period. Because of this, the period was found manually, by inspection of the data while varying the period on which it was folded. A period of 0.3987525 days was found to best overlay all of the R data, and the period was used to generate all of the R light curves in this paper. These data were again combined to form 35 phase bins, just like the B data, to lessen the scatter and aid the modeling. The periods of the plots for the B and V filters were not altered to this more precise period,

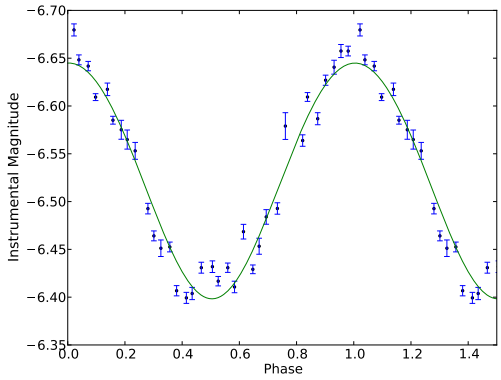

FIG. 2.— This is a sine curve fit to MACHO B data. This is shown to illustrate the slight non-sinusoidal shape of the light curve. The concave up portion of the data is too shallow and flat to be properly fit by a simple sine curve. The reduced chi square of this fit is 10.44.

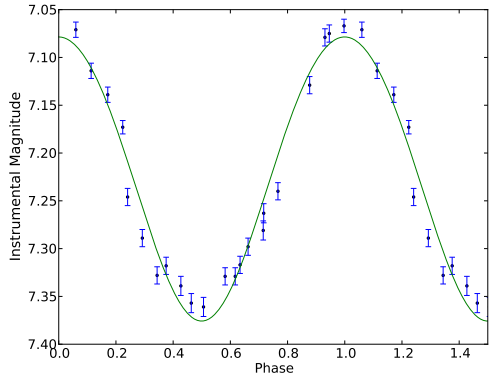

FIG. 3.— This is a sine curve fit to our V data. Clear deviation can be seen from perfectly sinusoidal behavior. Such deviation was instrumental in determining the lower limit for the inclination angle of the system. The reduced chi square of this fit is 5.92.

because, as the B and V filters contained data ranging over a much shorter baseline, the small change in period negligibly affected the shape of the plots.

3. EPHEMERIS

Because we had access to data from a longer base line than that which was previously published, we were able to refine the determination of the period of the system. This was performed using only R data, because the R data set had a significantly longer baseline than any other filter. The new ephemeris is given below, in JD.

$$T = 2454971.35(1) + 0.3987525(5)E.$$

The zero point given is the last time the system was observed to be at minimum light.

4. ANALYSIS

4.1. *Binary Maker 3*

All modeling of the target was performed with the software Binary Maker 3. Much effort was put into exploring the parameter space in its entirety. The parameter space was first searched with a broad grid pattern varying parameters systematically. The results of this grid search were then compared to our light curve data to determine the specific areas of parameter space that needed to be

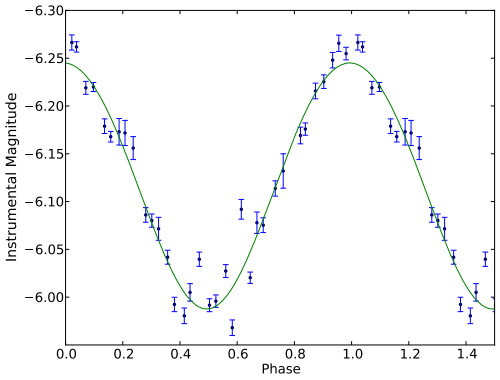

FIG. 4.— This is a sine curve fit to the R data. Though this filter shows greater scatter at minimum light than the other two filters, the light curve is still not as well fit by a sine curve as can be fit with our models. The reduced chi square of this fit is 7.89.

explored more thoroughly. Throughout modeling, our system was kept in a fairly simple state. The stars were assumed to be in a circular orbit. No spots were used, and limb darkening values were constrained to typical values for stars, between 0 and 1. The albedo coefficient was maintained at 1.0 for any star modeled with an effective temperature greater then 7200 K and 0.5 for cooler stars. This is assuming a sharp delimination between radiative and convective stars at this temperature. Finally, the stars were also assumed to rotate synchronously with their orbital period. The parameters that were varied are described in more detail below. The explanation of the effects of a parameter upon the synthetic light curve is relevant primarily to the parameter space that was explored most thoroughly, i.e. the parameter space near that where solutions to our light curves were found. They are not intended to describe the effects of these parameters in all possible situations.

4.1.1. *Temperature*

The temperature of the two stars, denoted as T_1 and T_2 in this report, is the effective surface temperature each star must have to match its light output continuum to a theoretical blackbody curve. In our analysis and report, a subscript of 1 refers to the hotter star and 2 refers to the cooler component. If an eclipsing light curve is evaluated, the ratio of the depths of the two eclipses is equal to the ratio of the temperatures of the two stars in the system. Our systems have been modeled to vary primarily through the irradiation effect. The hot progenitor of the planetary nebula heats up the near hemisphere of its cooler companion star, and the light of the system, as seen by us, varies as the hot hemisphere of the companion star rotates more or less into our view. As the T_1 is increased, the amplitude of the variation is also increased, because the temperature difference between the hot and cool hemispheres of the cooler star is increased. As one would then expect, increasing T_2 will cause the amplitude of the variation to decrease. The possible combinations of temperature values can be well constrained by observing a target at multiple wavelengths. The combination of T_1 and T_2 set the temperature of the hot hemisphere of the cool star, and thus they set the peak wavelength of light emitted by the hot hemisphere. This causes the amplitude of the variation

to change with wavelength. This leads to a fairly narrow range of temperatures that can successfully model photometric variability observed at three or more wavelengths.

4.1.2. *Inclination angle*

The inclination angle (i) is defined as the angle that the orbital plane of the binary system makes with the plane of the sky, as seen from our vantage point here on Earth. The variable i ranges from 0° to 90°. At $i = 90°$, the orbital plane is seen as edge on, and the binary system goes through eclipses from our point of view. At $i = 0°$, a circular orbit is projected as a perfect circle on the sky, and no photometric variability will be observed. As one increases i from 0° to 25° the amplitude of variability due to the irradiation effect steadily increases. Beyond $i = 25°$, the amplitude of the variability increases ever more slowly, but the concave up portion of the light curve flattens and broadens, deviating from a sine curve.

4.1.3. *Radii*

The parameters used to evaluate radii in Binary Maker 3 are equivalent to the Wilson - Devinney parameters r_1(back) and r_2(back). Physically, this represents the radius of a star as measured from the center of mass of the star to the point on the surface directly opposite the center of mass of the binary system, divided by the orbital separation of the system. Varying r_1(back) and r_2(back) has a drastic effect on the amplitude of variation in the light curves. In the parameter space that we found the system of Hf 2-2 to exist in, decreasing r_1(back) or incresaing r_2(back) leads to a greater amplitude of variation. In addition, a smaller r_1(back) tends to produce a flatter concave up portion of the light curve for a given inclination angle. Also, radii that are sufficiently large allow gravitational attraction between the two stars in the system to deform the stars from the typical spherical shape. This can dramatically change the shape of the light curve, as the surface area of the companion star visible to us is no longer constant. This produces higher data points around the 0.25 and 0.75 phases, where more of the elongated surface area is visible to us, giving the peak the appearance of shoulders. This effect is referred to as ellipsoidal variability.

4.1.4. *Mass Ratio*

The mass ratio is, quite simply, M_2 divided by M_1. The mass ratio determines the separation distance between the centers of mass of the stars in the system. Increasing the mass ratio beyond 1 increases the separation distance for a given orbital period. This, in turn decreases the amplitude of photometric variation, for the cooler star recieves less radiation from the hot star at greater distance. However, varying the mass ratio from 1 to 5 has a nearly neglible effect upon the amplitude of variation, so this parameter cannot be well-constrained by our modeling technique.

4.1.5. *Limb Darkening*

Binary Maker 3 uses a linear law of limb darkening, shown in the equation below. In the equation, θ is the angle measured between two vectors whose origin is the star center. One vector points toward the observer. It is 0° at the center of the star and 90° at the limb.

$$I(\theta) = I(0°)[1 - x + x\cos(\theta)]$$

The limb darkening value effects the extent to which surface brightness drops off as the line of sight moves from the bright center of the star to the edges. The limb darkening value for the cooler, larger star, x_2, can rather dramatically affect the shape of the curve. When dealing with the irradiation effect, increasing the value of x_2 causes the concave up portion of the light curve to become broader and flatter at the bottom. Decreasing the value will have the opposite effect. An increase in the limb darkening will also slightly increase the amplitude of the variation. A change of x_2 from 0.1 to 0.8, for example, would increase the amplitude of variation by as much as 5%.

4.2. *Details of Hf 2-2 Modeling*

The light curve of Hf 2-2 showed slight non-sinusoidal behavior. To illustrate this, Figures 2, 3, and 4 show the data in the various filters fit with a simple sine curve. These figures show how the concave up portion of each light curve is wider and flatter than a sine curve. This was instrumental in establishing the minimum angle of inclination with which we could model the system, for at low inclination angles, it is very challenging to introduce any non-sinusoidal behavior into the model. In the modeling, it was found that a rather large radius, 0.10 - 0.27 of the orbital seperation, was necessary for the central star in order to match the amplitude of variation seen in our data with a companion star of reasonable radius. The upper limit to the inclination was set by the lack of eclipses or ellipsoidal variability seen in our data, as well as the width of the concave up portion of the curve.

The temperature of the central star, T_1 was set at 67,000 K (Liu et al. 2006). T_2 was determined from the different amplitudes of variation in the B, V and R data. The width of the range in the possible temperatures is set primarily by the effect that limb darkening of the companion has on the amplitude of variation. The value of limb darkening for the central star had no significant effect on the light curve, but the value for the companion was allowed to wander between 0 and 0.8. As the true value is not known, and this value can vary at different wavelengths, this considerably broadened the possible temperature range for the companion star. If tighter limits can be set on the limb darkening of the companion star, the range of T_2 will be similarly more constrained.

The maximum radius of each star was limited by the lack of ellipsoidal variability in our data. To maintain the proper amplitude of variation, both stellar radii had to be increased at the same time. At large enough radii, the ellipsoidal variability makes the shape of the synthetic data clearly deviate from our observed data, setting the upper bound for the radii. The minimum radii could not be established by this modeling procedure. Decreasing both radii at the same time, it is possible to continue to reproduce our data at radii far smaller than are likely to physically exist, given our knowledge of the nature of stars.

TABLE 1
Overall Constraints

Parameter	Range
T_2	4000 K - 8500 K
r_1(back)	$\leq$ 0.27 a
r_2(back)	$\leq$ 0.36 a
M_2	$\leq 1.3 M_\odot$
Mass Ratio	$\leq$ 2.4
i	25° - 55°

TABLE 2
Inclination = 25°

Parameter	Range
T_2	4000 K - 8500 K
r_1(back)	$\leq$ 0.12 a
r_2(back)	$\leq$ 0.3 a
M_2	$\leq 1\ M_\odot$
Mass Ratio	$\leq$ 1.8

TABLE 3
Inclination = 32.5°

Parameter	Range
T_2	5000 K - 8500 K
r_1(back)	$\leq$ 0.21 a
r_2(back)	$\leq$ 0.35 a
M_2	$\leq 1.3\ M_\odot$
Mass Ratio	$\leq$ 2.4

TABLE 4
Inclination = 40°

Parameter	Range
T_2	6000 K - 8500 K
r_1(back)	$\leq$ 0.265 a
r_2(back)	$\leq$ 0.36 a
M_2	$\leq 1.3\ M_\odot$
Mass Ratio	$\leq$ 2.4

TABLE 5
Inclination = 47.5°

Parameter	Range
T_2	6500 K - 8000 K
r_1(back)	$\leq$ 0.27 a
r_2(back)	$\leq$ 0.33 a
M_2	$\leq 1.2\ M_\odot$
Mass Ratio	$\leq$ 2.2

5. RESULTS

A summary of system parameters, constraints derived from the modeling, are given in tables 1 through 6. Table 1 shows the overall constraints for the system. Tables 2 through 6 show the constraints if the system were known to be at a specific inclination angle, as the constraints of some parameters are quite dependent upon the inclination of the system. In the tables, radii are given as a fraction of the orbital seperation, a. The subscript 1 corresponds to the central star of the nebula, while the subscript 2 corresponds to the cooler companion star.

TABLE 6
Inclination = 55°

Parameter	Range
T_2	7000 K - 8500 K
r_1(back)	$\leq$ 0.265 a
r_2(back)	$\leq$ 0.31 a
M_2	$\leq 1\ M_\odot$
Mass Ratio	$\leq$ 1.8

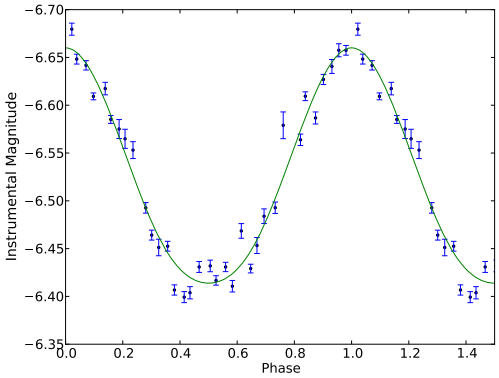

Fig. 5.— This is a sample model to MACHO B data. In this model, T_1 =67,000K and T_2 =7,500K. The modeled mass ratio is 1.7. r_1(back)= 0.16 and r_1(back)= 0.28 This is modeled at i=40$^\odot$

The upper limit to the mass of the companion star and the mass ratio were not determined directly from the modeling but rather are a logical extension of the modeling. This is most easily illustrated by example, so we'll step through the derivation of the mass ratio and the mass of the companion at an inclination angle of 25°.

First, it is important to understand that close binary companions of PN progenitor stars are usually found to be hotter and larger than their main sequence counter parts, for a given mass. This makes sense as the companion star is being heated by the hot central star. A hotter star will tend to expand a bit, to maintain hydrostatic equilibrium throughout its structure. Thus, for a given mass, the main sequence values for temperature and radius are treated as good lower limits. More useful for this derivation is the idea that for a given temperature or radius, the corresponding main sequence mass can be treated as an upper limit. A progenitor star of a PN, like our central star, should be in the range between $0.55M_\odot$ and $1.4M_\odot$. Below this range, the star is unlikely to ever get hot enough to photoionize the surrounding gases to form a nebula. Above this mass, a non-fusing star would collapse into a neutron star. At $i = 25°$, the maximum temperature for the companion star is 8,500K. This corresponds to a main sequence mass of about $2M_\odot$ (Gray 2005). To maximize orbital seperation, we'll assume a central star mass of $1.4M_\odot$. With a period of 0.39874 days, this gives a maximum orbital seperation of $3.8R_\odot$. As the maximum value of r_2(back) is 0.3, the maximum radius of the companion is 1.14 $R_\odot$. Again, using the main sequence as an upper limit to the mass, this corresponds to a star of about $1.2M_\odot$. This new mass is then used to calculate the maximum orbital seperation with our given period and a PN central star companion. This iteration will yield a maximum stellar radius of $1.05R_\odot$.

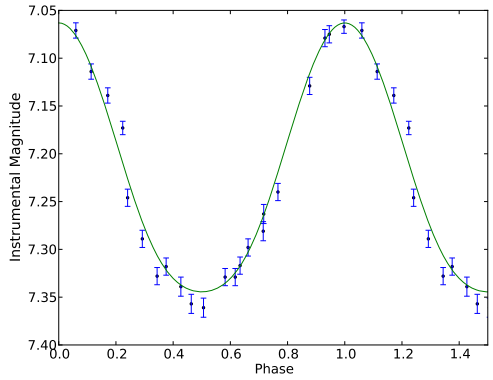

FIG. 6.— This is a sample model of the system fit to our V data. This model uses the same parameters as that in Figure 5

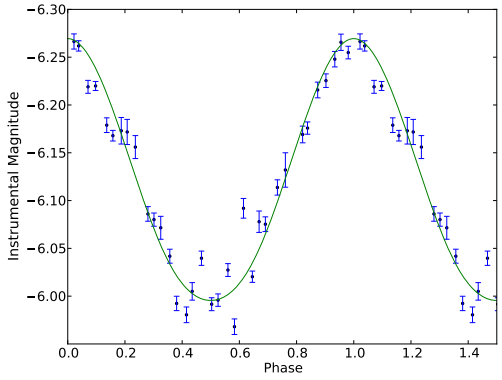

FIG. 7.— This is a sample model of the system fit to our R data combined with that from the MACHO survey. This model uses the same parameters as that in Figure 5

Further iterations settle down to a stellar companion of less than or equal to $1.0M_{\odot}$. As the minimum mass of our central star is about $0.55M_{\odot}$, this yields a maximum mass ratio of 1.8. This process was repeated at all of the inclination angles listed in tables 2-5.

Sample models are fit to the light curve data in Figures 5-7. As all of the models within the constrained parameter space solve the light curve approximately equally well, all of the possible models display quite similar behavior. The sample models are representative of the shape of all the solutions to the light curves in the constrained parameter space.

6. CONCLUSIONS

We have constrained the parameters of the binary central star of Hf 2-2 as much as possible with the currently available data. The lower limit on the inclination of Hf 2-2 can be very useful in supporting or refuting the hypothesis that binary stars shape PNe, once the nebular structure is properly studied. From visual inspection of the nebula in Figure 1, a preliminary conclusion can be drawn that the range of possible inclinations of the binary system includes agreement with the nebula. It is hoped that the results of this study can be combined with studies modeling many other binary central stars. In this way, it can be determined if there exists a statistically significant correlation between inclination angles of binary systems and the axes of the planetary nebulae that form around them.

This project was funded by the National Science Foundation Research Experiences for Undergraduates (REU) program through grant NSF AST-1004872. This paper utilizes public domain data obtained by the MACHO Project, jointly funded by the US Department of Energy through the University of California, Lawrence Livermore National Laboratory under contract No. W-7405-Eng-48, by the National Science Foundation through the Center for Particle Astrophysics of the University of California under cooperative agreement AST-8809616, and by the Mount Stromlo and Siding Spring Observatory, part of the Australian National University.

REFERENCES

Balick, B., & Frank, A. 2002, ARA&A, 40, 439
Bond, H., & Murdin, P. 2000, Encyclopedia of Astronomy and Astrophysics,
De Marco, O., Hillwig, T. C., & Smith, A. J. 2008, AJ, 136, 323
De Marco, O. 2009, PASP, 121, 316
Frank, A., Balick, B., & Riley, J. 1990, AJ, 100, 1903
Frew, D. 2008, Planetary Nebulae in the Solar Neighbourhood: Statistics, Distance Scale and Luminsosity Function [dissertation],Sydney, Macquarie University
Gray, David F. 2005, THe Observation and Analysis of Stellar Photospheres; New York: Cambridge University Press
Hoffleit, D. 1953, Annals of Harvard College Observatory, 119, 37
Kwok, S., Purton, C. R., & Fitzgerald, P. M. 1978, ApJ, 219, L125
Kwok, S., Hrivnak, B. J., & Su, K. Y. L. 2000, ApJ, 544, L149
Kwok, S. 2007 "'The Origin and Evolution of Planetary Nebulae"', Cambridge Astrophysics Series No. 33, Cambridge University Press.
Liu, X.-W. 2003, Planetary Nebulae: Their Evolution and Role in the Universe, 209, 339
Liu, X.-W., Barlow, M. J.,
Lutz, J., et al. 1998, Bulletin of the American Astronomical Society, 30, 894
Miszalski, B., Acker, A., Moffat, A. F. J., Parker, Q. A., & Udalski, A. 2009, A&A, 496, 813
Schaub, S. C., & Hillwig, T. 2009, Bulletin of the American Astronomical Society, 41, 462
Schwarz, H. E., Corradi, R. L. M., & Melnick, J. 1992, A&AS, 96, 23
Stasińska, G., Fresneau, A., da Silva Gameiro, G. F., & Acker, A. 1991, A&A, 252, 762 Zhang, Y., Bastin, R. J., & Storey, P. J. 2006, MNRAS, 368, 1959